Interpenetrating Liquid Crystal Elastomer and Ionogel as Tunable Electroactive Actuators and Sensors

Yakui Deng, Gaoyu Liu, Annie Brûlet, Giao T M Nguyen, Daniel Dudzinski, Frédéric Vidal, Cédric Plesse, Cédric Vancaeyzeele, Min-hui Li

ADVANCED FUNCTIONAL MATERIALS
www.afm-journal.de

Interpenetrating Liquid Crystal Elastomer and Ionogel as Tunable Electroactive Actuators and Sensors

Yakui Deng, Gaoyu Liu, Annie Brûlet, Giao T. M. Nguyen, Daniel Dudzinski, Frédéric Vidal, Cédric Plesse, Cédric Vancaeyzeele, and Min-Hui Li**

Electroactive liquid crystal elastomers (eLCEs) are used to make actuators and soft robotics. However, most eLCEs are monofunctional with one type of deformation (bending or contraction). Recently, a trilayer eLCE are reported by combining ion-conducting LCE and ionic electroactive polymer device (i-EAD). This i-EAD-LCE is bifunctional and performs either bending or contractile deformation by controlling low-voltage stimulation. Nevertheless, it has a Young's modulus of only 1.63 MPa. To improve the mechanical performance, the i-EAD-IPN-LCE is prepared here, whose central membrane is composed of interpenetrating LCE and ionogel (i-IPN-LCE) instead of a single ion-conducting LCE. This i-EAD-IPN-LCE with a typical thickness of 0.5 mm can function not only as linear and bending actuators, but also as a sensor. As a linear actuator, its Young's modulus, actuation stress, and strain are 51.6 MPa, 0.14 MPa and 9%, respectively, reaching skeletal muscles' values. As a bending actuator, its bending strain difference $\Delta\epsilon$ is 1.18% with 3 mN output force. It can also operate as a sensor producing 0.4 mV Open-Circuit-Voltage to respond to bending deformation ($\Delta\epsilon = 9\%$). Therefore, this i-EAD-IPN-LCE is a promising system for the fabrication of robust electroactive devices and sensors with multiple degrees of freedom.

1. Introduction

Over the past few decades, stimuli-responsive smart materials have been successfully developed in the context of artificial muscles, artificial skins, or soft robotics.[1,2] Liquid crystal elastomers (LCEs) belong to this category of smart materials, which can produce extremely sensitive deformations in response to various external stimuli such as heat and light.[3–16] Especially, the uniformly ordered nematic LCEs possess fascinating features combining the entropic elasticity of elastomers and the reversible and alignment-dependent shape-change behavior of liquid crystal polymers (LCPs) through LC phase transition.[17–20] Although temperature change and light irradiation are the most used stimuli for LCEs, electrical energy is the most convenient and the most in demand stimuli, especially for portable devices and soft robotics. Electroactive LCEs (eLCEs) have thus attracted the attention of more and more researchers. The most studied method is the electrothermal one by introducing the Joule effect into LCEs. For example, the incorporation of electron-conducting materials like nanomaterials,[21] metal wires,[22,23] or liquid metals[24,25] within the LCE can produce Joule heating controlled by an electric current. Another way to introduce Joule heating control relies on alternative ionic current, which can be enabled when an ion-conducting LCE film is prepared and sandwiched between two compliant electrodes, i.e., designed as an ionic electroactive polymer device (i-EAD).[26] Normally for operation in open air, the traditional i-EAD is composed of an ion-conducting polymer (ICP) sandwiched between two electron-conducting polymer (ECP) layers. This trilayer device (ECP/ICP/ECP) converts either electrical stimulation into reversible large bending deformation (actuator) or mechanical stimulation into electrical signal (sensor) owing to the low driving voltages.[27–30] Our groups recently reported a bifunctional i-EAD-LCE system, where the ICP is an ion-conducting LCE and the ECP is made of formulated PEDOT:PSS.[26] This i-EAD-LCE can contract or bend on-demand depending on the electrical stimulation, thanks to its trilayer configuration. Under AC electrical stimulation, fast back and forth motions of ions between the compliant electrodes promote bulk Joule heating and trigger the nematic-isotropic transition of the LCE, thus

Y. Deng, G. Liu, M.-H. Li
Chimie ParisTech
Institut de Recherche de Chimie Paris
Université Paris Sciences & Lettres
CNRS
UMR8247, 11 rue Pierre et Marie Curie, Paris 75005, France
E-mail: min-hui.li@chimieparistech.psl.eu

A. Brûlet, D. Dudzinski
Laboratoire Léon Brillouin
Université Paris-Saclay
UMR12 CEA-CNRS, CEA Saclay, 3 rue Joliot Curie, Gif sur Yvette cedex 91191, France

G. T. M. Nguyen, F. Vidal, C. Plesse, C. Vancaeyzeele
Laboratoire de Physicochimie des Polymères et des Interfaces (LPPI)
CY Cergy Paris Université
5 mail Gay Lussac, Cergy-Pontoise Cedex 95031, France
E-mail: cedric.vancaeyzeele@cyu.fr

The ORCID identification number(s) for the author(s) of this article can be found under https://doi.org/10.1002/adfm.202403892

DOI: 10.1002/adfm.202403892

leading linear.contraction. Meanwhile, because electrodes are themselves electromechanically active, such i-EAD-LCE system can bend under DC electrical stimulation thanks to the electrochemical charging/discharging and associated volume variation of the PEDOT:PSS electrodes. However, since the ion-conducting LCE reported showed limited mechanical performance,[26] the i-EAD-LCE had a Young's modulus of only 1.63 MPa and was too soft to measure the actuation stress by any mechanical stress/strain sensor, while mammalian skeletal muscles have much higher Young's modulus (10–60 MPa) and actuation stress (0.1–0.35 MPa).[31,32] Besides, the function of sensor had not been observed. Therefore, improving the mechanical properties of the LCE layer is crucial for the development of a robust trilayer eLCE as actuator and sensor. For this purpose, we fabricate here ion-conducting LCE membranes with interpenetrating polymer networks, named as i-IPN-LCE. The interpenetrating polymer network (IPN) with physically interlaced networks have been reported as an efficient way to enhance the mechanical properties of polymer networks.[33,34] The IPN concept has already been introduced in LCE field by several groups,[35–44] who have developed IPNs of liquid crystal elastomers (IPN-LCEs) or liquid crystal hydrogels as smart materials and biosensors. Especially, the IPN-LCEs composed of a polyurethane-based LCE and a polyacrylate-based LCE reported by Yang and co-workers[42] exhibit ultra-strong mechanical properties with an elastic Young's modulus of 10.4 MPa and an actuation stress of 2.53 MPa. In this work, the i-IPN-LCE is prepared not only for the mechanical properties, but also for the integration of the desired functional properties from each polymer network, i.e., stimuli-responsive properties from the aligned LCE and ionic motions from the robust ionogel.

There are generally two strategies to prepare IPN. The first one uses the sequential polymerizations: one network is first prepared and swollen by the second monomer; then the polymerization of the second monomer is carried out to form the second network.[35–41] The second strategy uses orthogonal reactions to polymerize the two monomers at the same time so that both networks can be simultaneously formed from a uniform mixture of monomers.[42–44] For the sake of mechanical properties, the first strategy is less advantageous, because the swelling treatment might disrupt the chain anisotropy of LCE that should be prepared first and also cause a non-uniform dispersion of the second monomer in the LCE. Therefore, we adopt the second strategy to prepare ion-conducting i-IPN-LCE by using polyurethane- and polyacrylate-based networks, because the urethane step-growth polymerization and acrylate chain-growth polymerization are orthogonal and do not interfere with each other.[42–44] Concretely, the two networks are respectively polyurethane LCE and polyacrylate ionogel with poly(ethylene glycol) (PEG) side-chain and ionic liquid (IL) ($EMIM^+$ $TFSI^-$: 1-ethyl-3-methylimidazolium bis(trifluoromethylsulfonyl)imide) (**Figure 1a**). This type of ionogel has already been used successfully by one of our groups in electroactive nitrile butadiene rubber IPN actuators[45,46] and an electroactive shape-memory IPN.[47]

The i-IPN-LCE membrane is further integrated in the trilayer configuration with two ECP electrodes made of formulated PEDOT:PSS to get the final device i-EAD-IPN-LCE (Figure 1b) as described previously.[26] Under low-voltage stimulation, the i-EAD-IPN-LCE can perform bending or contractile deformations depending on frequency and voltage (Figure 1c). The mechanical performance of this i-EAD-IPN-LCE actuator has been largely improved compared to the previous i-EAD-LCE system.[26] As a linear actuator, the i-EAD-IPN-LCE has a Young's modulus of 51.6 MPa and an actuation stress of 0.14 MPa, that are in the range of the values of mammalian skeletal muscles. As a bending actuator, the bending strain difference has also been increased and an output force measured. Moreover, the i-EAD-IPN-LCE can operate as a sensor that produce electrical signals in response to bending deformations (Figure 1d). Therefore, due to the improved mechanical performance, this i-EAD-IPN-LCE with interpenetrating LCE and ionogel is a promising system for the fabrication of robust electroactive devices and mechanical sensors with multiple degrees of freedom.

2. Results and Discussion

2.1. Interpenetrating LCE and Ionogel with Ion-Conductivity (i-IPN-LCE)

The chemicals for the preparation of polyurethane LCE and polyacrylate ionogel are shown in Figure 1a. The hydroxyl terminated LC monomer (2-methyl-1,4-phenylene bis(4-((6-hydroxyhexyl)oxy)benzoate)) was first synthesized. Synthesis and characterization details are given in Supporting Information. The polyurethane LCE was obtained by the polyaddition of the diol groups in the LC monomer with the tri-isocyanate groups in the cross-linker Desmodur N3300 catalyzed by dibutyltin dilaurate (DBTDL). The polyacrylate ionogel was formed from free-radical copolymerization of poly(ethylene glycol) methyl ether acrylate (PEGA) and poly(ethylene glycol) diacrylate (PEGDA) in the presence of ionic liquid (IL: EMIM TFSI), using Irgacure 369 as photoinitiator. The preparation procedure of i-IPN-LCE is schematically illustrated in Scheme S1 (Supporting Information) and described in detail in Supporting Information. Typically, a homogenous mixture of all components, i.e., the precursors of two networks and the ionic liquid, (Figure 1a) dissolved in DMF was added into a polytetrafluoroethylene (PTFE) mold sandwiched between two glass plates. The mold was first placed in an oven at 50 °C for 1.5 h to obtain a partially cross-linked LC polyurethane network. The sample was then irradiated under UV light for a short period (5 s) to get a partially cross-linked PEG polyacrylate network. The sample film was then peeled off the mold and dried in a vacuum oven at 50 °C for 1.5 h to remove most of DMF. During this drying process, polyaddition to form urethane bonds should continue. After drying, the intermediate sample was stretched to 150% of its original length by a tensile machine to align the LC polymer chains. While keeping the stretched state, the sample film was irradiated by UV light on both sides (each side for 5 min) to complete photo-cross-linking of the PEG polyacrylate network. Finally, a monodomain film of i-IPN-LCE was obtained.

To find a good balance between the contraction ratio of LCE and the ionic conductivity of ionogel, different molar ratios of LC monomer to PEG acrylate monomers (PEGA and PEGDA), simply noted as LC:PEG, have been used in the preparation of i-IPN-LCE. With LC:PEG = 30:70, 40:60, 50:50, 60:40, and 70:30, a series of samples named as IPN1, IPN2, IPN3, IPN4, and IPN5 was obtained, respectively (see Table S1, Supporting Information).

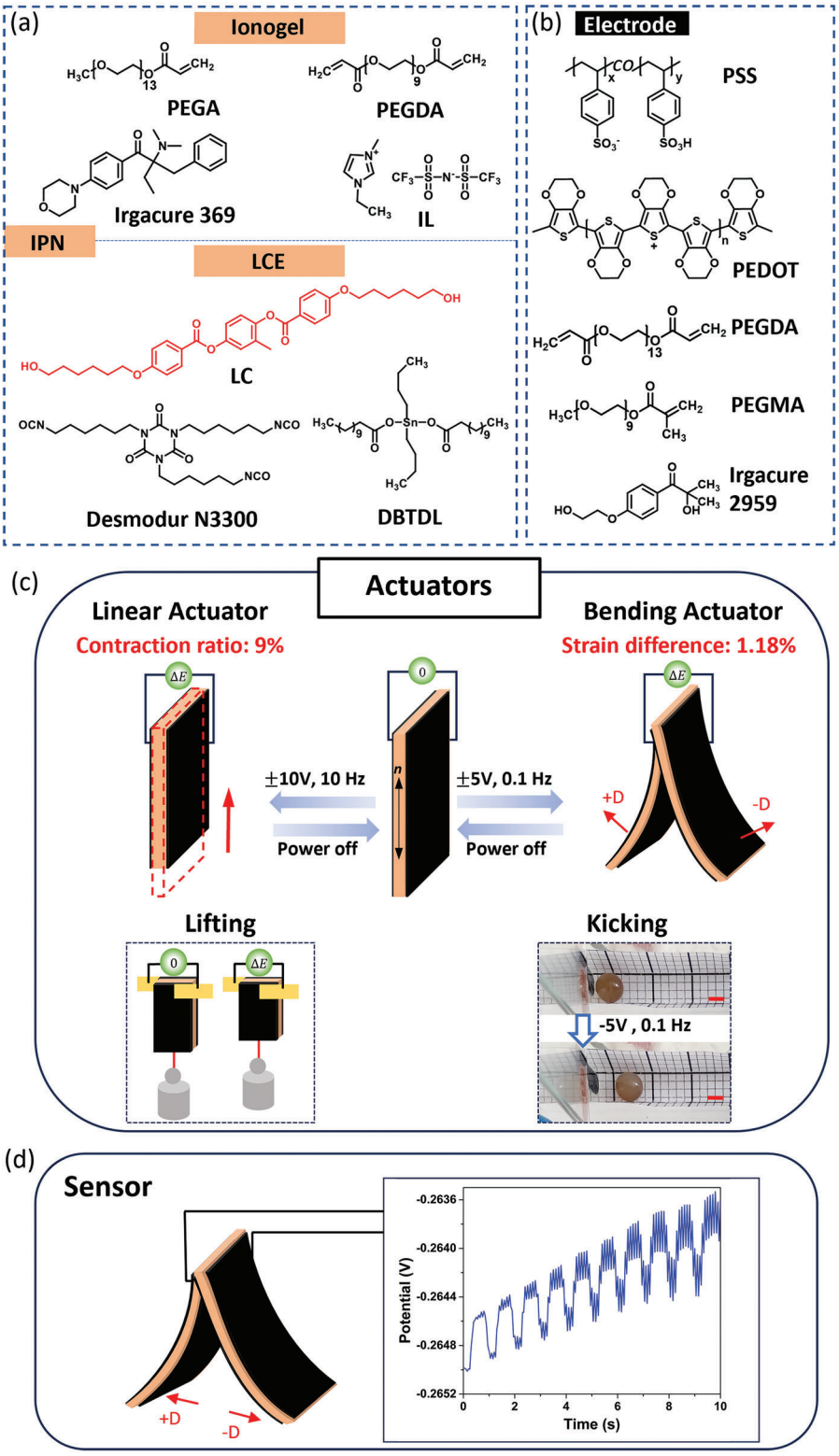

Figure 1. a) Chemical structures of the components to make i-IPN-LCE (ionogel network/LCE network) film. b) Chemical structures of the components to make the formulated PEDOT:PSS electrodes. c) The trilayer i-EAD-IPN-LCE as electroactive actuator and bending sensor. The orange central layer represents the ion-conducting i-IPN-LCE film (*n* indicating the nematic alignment direction), while the two black side layers represent the formulated PEDOT:PSS electrodes. Depending on the applied electrical voltage and frequency, the i-EAD-IPN-LCE performs either linear contraction deformation or bending deformation. It can work as a robotic arm to lift a load, or mimic the Golf shot to kick a ball (top view, scale bar = 4 mm). d) The i-EAD-IPN-LCE can also convert mechanical bending to electrical signals as a sensor.

For each sample, the molar ratio of PEGA to PEGDA was 1:2, and the weight proportion of IL versus PEG acrylate monomers was kept at 1:1. In addition, single networks of LCE and ionogel (LC:PEG = 100:0 and 0:100) were also prepared for comparison (see Supporting Information for details). FT-IR spectra were performed to analyze the conversion of different functional groups during the preparation of IPN1-5 as shown in Figures S1–S5 (Supporting Information). Taking IPN2 as an example (Figure S1, Supporting Information), it is interesting to note that all signals of —N=C=O groups (≈2260 cm^{-1}) disappeared already in the intermediate sample, which means the cross-linking of PU network was completed before mechanical stretching for alignment. In contrast, acrylic —C=C— signals (≈1388 cm^{-1}) survived in the intermediated sample and disappeared in the final IPN2. The same results were observed in IPN1, IPN3, IPN4, and IPN5 (Figures S2–S5, Supporting Information). Therefore, the alignment of the LCE was finally locked by the complete cross-linking of polyacrylate network (ionogel) during the second UV irradiation step. To further confirm the efficiency of orthogonal cross-linking reactions, PEG polyacrylate network, LCE PU network and IPN with LC:PEG = 40:60, all in the absence of IL, were also prepared in the same conditions. After Soxhlet extraction (see Supporting Information for detail), the extractible contents (EC) were 10%, 4%, and 10%, respectively, showing a small amount of unreacted starting material in each case. The cross-linking reactions simultaneously applied to prepare IPN did not significantly affect their efficiency since the EC of IPN with LC:PEG = 40:60 (10%) was closed to the weighted EC (7.6%) calculated from the values of PEG polyacrylate network and LCE PU network.

2.1.1. Liquid Crystal Properties and Thermal Actuations of i-IPN-LCE

The liquid crystal properties of the i-IPN-LCE with interpenetrating LCE and ionogel were then studied using polarized optical microscopy (POM), differential scanning calorimetry (DSC) and 2D wide and small angle X-ray scattering (2D-WAXS and SAXS). Taking IPN2 as an example, **Figure** 2a shows its typical POM images in aligned state. The light transmission of the IPN2 sample placed with alignment direction (***n***) parallel to polarizer (**p**) was clearly different from the sample placed with ***n*** tilted at 45° relative to **p**. This clearly demonstrates the existence of anisotropy. DSC measurement (Figure S6, Supporting Information) shows glass transition temperature (T_g) of PEO and LCE at −45 and 18 °C, respectively (on heating), and a bump signal between 50–100 °C for the domain of nematic-isotropic (N-I) transition.

Figure 2b shows the 2D-WAXS pattern of IPN2 that is clearly anisotropic and the crescent-like signal (at q = 1.43 $Å^{-1}$) along the alignment direction allows to calculate the nematic order parameter S[48] (see Supporting Information for details), here S = 0.59 for IPN2 at 25 °C. In this 2D-WAXS pattern at low q (near the beam trap), two peaks at q = 0.117 $Å^{-1}$ parallel to the alignment direction are also visible (indicated by two black arrows), which correspond to the LC repeat unit of 5.37 nm in the aligned nematic phase. 2D-WAXS was then recorded as a function of temperature upon heating to explore the evolution of the order parameter S. As shown in Figure S7a (Supporting Information), the S value started to decrease continuously from S = 0.59 at 55 °C to S = 0.28 at 130 °C without a clear crossover as in the single network of ion-conducting LCE previously reported.[26] The same result was also obtained in IPN3 (Figure S7b, Supporting Information). This phenomenon is consistent with the broad domain of N-I transition detected by DSC. Moreover, some anisotropic order still existed beyond T_{NI} (S = 0.28 at 130 °C). This observation can be explained by the cross-linked nature of the material that may prevent full relaxation toward the isotropic disordered state. Note that the chain elongation in the ionogel by mechanical stretching also contribute to the anisotropy of the crescent signals. However, this part of anisotropy should not be reversible, thus the S values during the second heating from 25 to 130 °C are lower than those during the first heating as shown in Figure S7b (Supporting Information).

The 2D-SAXS patterns of IPN2 recorded in q = 0.01 – 0.2 $Å^{-1}$ as shown in Figure 2c confirms the facts that some anisotropic order still exists beyond T_{NI} and that a part of anisotropy in the sample is not reversible when the temperature returns to 25 °C after the 1st heating/cooling cycle. In Figure 2c the two peaks at q = 0.117 $Å^{-1}$ parallel to the alignment direction (again indicated by two black arrows) are intense at 25 °C. They become weaker at 65 °C and finally disappear at 105 °C. That means the N-I transition ends before 105 °C. However, the very small q scattering signal retains an oval form at all temperature, even in the isotropic phase at 105 °C. The SAXS intensity profile in this small q range (q = 0.025 – 0.08 $Å^{-1}$) quantitatively shows the anisotropy of IPN2 on the 1st heating and cooling process (Figure S8, Supporting Information). The anisotropic value is determined by the ratio $q_{\perp}/q_{//}$ at a given intensity (for example I = 0.25 a.u. in Figure S8, Supporting Information), where $q_{\perp}$ and $q_{//}$ are the scattering vectors in the direction perpendicular and parallel to the alignment direction. On the 1st heating cycle, the anisotropic value is $q_{\perp}/q_{//}$ = 1.33 at 25 °C for the pristine IPN2 and decreases down to 1.19 (but not 1) at 105 °C. After the 1st cooling back to 25 °C, the anisotropy value re-increases to 1.24. Interestingly, the anisotropy does not return to the initial value of 1.33 after the whole 1st heating/cooling cycle: ≈7% of anisotropy is not reversible. This observation can be explained by the alignment method and the existence of two interpenetrating networks. Indeed, during the preparation of monodomain i-IPN-LCE, the intermediate sample was mechanically stretched: the LC polymer chains in LCE network were orientated and the polymer chains of ionogel network were also elongated. In the final i-IPN-LCE, the orientations of both kinds of chains were locked by the second cross-linking. Upon the first heating to isotropic phase (105 °C, also superior to T_g of ionogel), the chain conformation of LCE changes from highly elongated to nearly isotropic and the elongation of PEO and polyacrylate chains in ionogel are also relaxed. However, only the chain conformation change in LCE is reversible upon temperature change (through N-I transition),[3] while that of amorphous chains in ionogel is not. Therefore, the anisotropy gained by chain stretching in the ionogel part will be lost after the first heating/cooling process.

Further, the thermal responsive contraction and elongation of all i-IPN-LCE samples, i.e., IPN1, IPN2, IPN3, IPN4, IPN5, were investigated. The mechanism of linear actuation of LCE resides in the chain conformation change of each individual LCP chain at LC-isotropic phase transition. In LCP, the LC order is closely coupled with the polymer chain conformation.[19] Due to this coupling, the nematic main-chain LCP shows a prolate

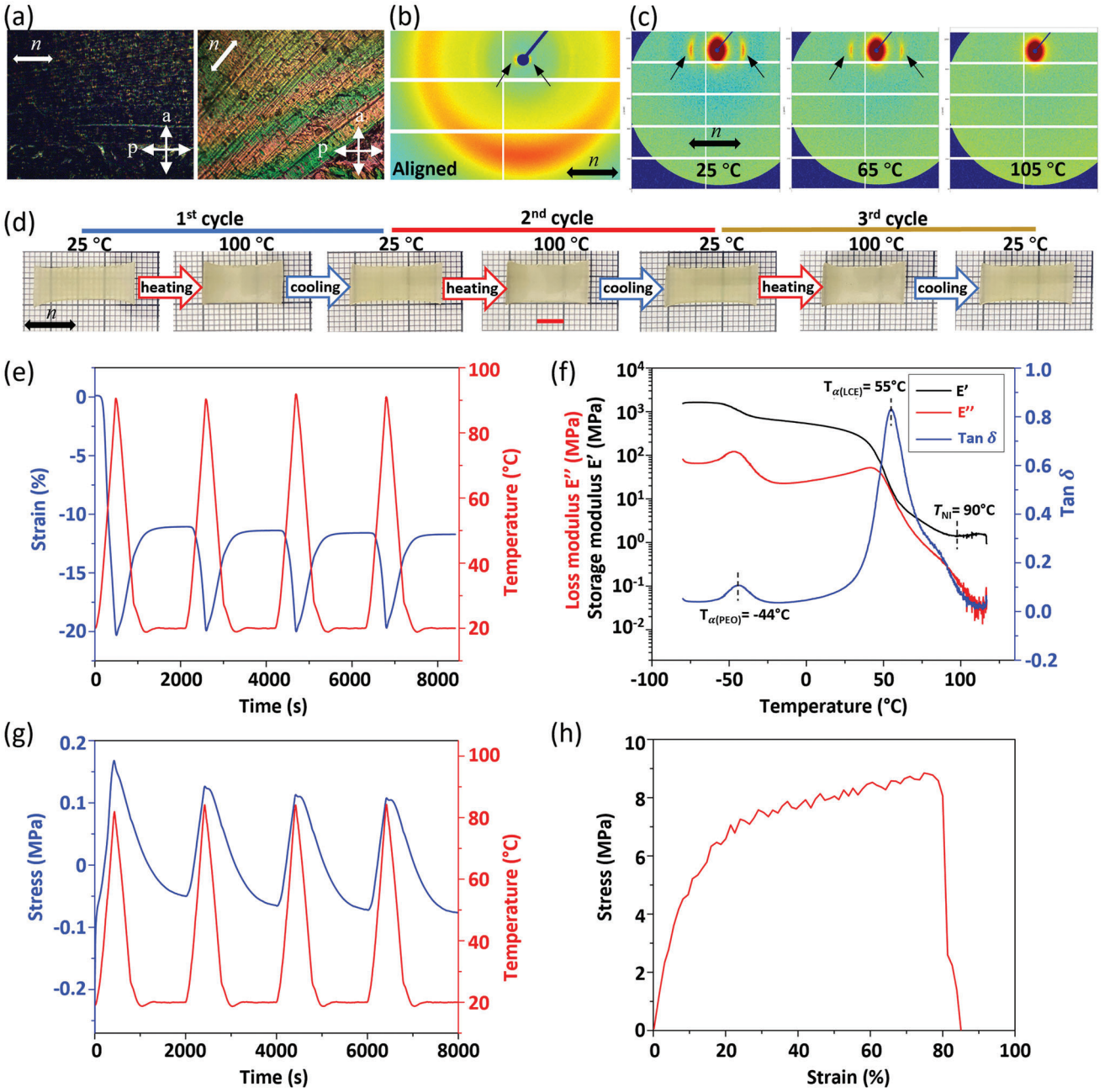

Figure 2. Characterization of the IPN2 film (LC:PEG = 40:60). a) Polarizing optical microscopic (POM) images with the alignment direction (***n***) either parallel (left) or tilt at an angle of $\theta = 45°$ (right) to the polarizer (p) (a indicating the second analyzer, called analyzer). b) 2D-WAXS patterns of IPN2 at 25 °C. c) 2D-SAXS patterns of IPN2 at 25, 65, and 105 °C. The nematic director (***n***) is along the stretching direction. d) Photographs of IPN2 film (length (l) × height (h) × thickness (w) = 19 × 6.5 × 0.57 mm, scale bar = 5 mm) upon 1st, 2nd, and 3rd heating and cooling cycles, with the maximal contraction observed at 100 °C. e) Thermal actuation strain measured at iso-stress mode by DMA (heating/cooling rate: ±3 °C min^{-1}, stress control: 0.02 N). f) Storage modulus (E'), loss modulus (E") and loss factor tan δ by DMA at temperature ramp mode (heating rate: 3 °C min^{-1}, strain control: 0.01%). g) Thermal actuation stress measured at iso-strain mode by DMA (heating/cooling rate: ±3 °C min^{-1}, strain control: 0.01%). h) The stress-strain diagram of IPN2 film measured by tensile machine at room temperature (25 C, strain rate:10 mm min^{-1}).

or even elongated cylindrical conformation, while its conformation is spherical in the isotropic (disordered) phase.[19] Upon heating the LC-isotropic (order-disorder) phase transition will cause the chain conformation changes from prolate to spherical, and each individual polymer chain will undergo a contraction in the direction of nematic director ***n***. This process is reversible, i.e., a chain elongation will take place upon cooling though isotropic-LC transition. In a monodomain LCE, all LCP chains are oriented in the same direction and the orientation is locked by cross-linking. Consequently, the conformational change of

individual polymer chain is just translated to the LCE to get the material contraction/elongation.[3,18] Here the thermoactivated contraction/elongation of IPN2 are effectively demonstrated by the photographs in Figure 2d showing the maximal contraction (T_{max} = 100 °C) and the maximal elongation (T_0 = 25 °C) upon three heating-cooling cycles from 25 °C to 150 °C. The linear contraction ratios are defined as $(L_0 - L)/L_0$, where L_0 is the film length at 25 °C at the beginning of each cycle, and L that at $T = T_{max}$. They were measured as 20%, 9%, and 9% for the 1st, 2nd, and 3rd cycles, respectively. That means the contraction/elongation during the 1st heating/cooling cycle is not totally reversible, while those during the subsequent 2nd and 3rd cycles are reversible. This phenomenon was observed for all IPN1-5 samples, whose contraction ratios are listed in Table S2 (Supporting Information). After the 1st heating/cooling cycle, the maximal reversible contraction ratios of IPN1, IPN3, IPN4, and IPN5 during the 2nd and 3rd heating/cooling cycles were measured as 0%, 12%, 13.5%, and 14%, respectively (Table S2, Supporting Information). IPN1 showed nonreversible contraction probably due to its low LC content.

The thermal actuation strain measured at iso-stress mode by dynamic mechanical analysis (DMA) (Figure 2e) confirms further the above observations. The macroscopic length variations during the first heating/cooling cycles are thus in good agreement with the SAXS results at molecular chain level discussed above. The uncomplete length recover after the first cycle is caused by the mechanical stretching alignment and the existence of two interpenetrating networks. Therefore, for actuator and sensor applications, the i-IPN-LCE film will not be used in pristine state, but should be submitted to an annealing treatment, i.e., a first heating/cooling cycle to $T = T_{max}$ and back to 25 °C, before its integration into the trilayer device as central ion-conducting component.

2.1.2. Ionic Conductivities of i-IPN-LCE and Mechanical Properties of IPN2

The ionic conductivities of all i-IPN-LCE samples (IPN1-5) were the subject of an in-depth study to choose an optimal sample as the central membrane for the preparation of trilayer i-EAD-IPN-LCE. The ionic conductivity (σ) of the single ionogel, IPN1, IPN2, IPN3, IPN4, IPN5 and the single LCE were measured by electrochemical impendence spectroscopy (EIS) in the temperature range of 20–70 °C (see Supporting Information for detail). As shown in Figure S9 and Table S3 (Supporting Information), among IPN2, IPN3, IPN4, IPN5, the IPN2 film exhibits the best ionic conductivity: at 20 °C σ (IPN2) = 3.4×10^{-5} S cm^{-1}, and at 70 °C σ (IPN2) = 1.9×10^{-4} S cm^{-1}. IPN1 shows even better ionic conductivity, but its reversible thermal contraction ratio is nearly null as discuss above. Finally, IPN2 was chosen for i-EAD-IPN-LCE preparation because of its good balance between thermal actuation strain and ionic conductivity.

The thermal stability of IPN2 was examined by thermogravimetric analysis (TGA) (Figure S10, Supporting Information). The degradation onset temperature corresponding to 5 wt.% loss ($T_{5\%}$) was measured as 295 °C, indicating a good thermal stability. The thermo-mechanical characterization of IPN2 by DMA (Figure 2f) shows a typical viscoelastic behavior with two α relaxation temperature (T_α) at −44 and 55 °C corresponding to the loss factor tan δ peaks. The two relaxations were assigned to PEO in the ionogel and to LCE. At the temperature ≈90 °C, the storage modulus increases upon heating. This is not a mechanical transition but the signature of the thermal contraction of LCE; therefore, it is the N-I transition.[26] The thermal actuation stress of IPN2 was measured at iso-strain mode by DMA (Figure 2g). The maximum actuation stress during the contractile stroke is 0.24 MPa during the 1st heating cycle, then it decreases and finally stabilizes to 0.16 MPa in the 2nd–4th cycles that are reversible actuation cycles. The quasi-static stress-strain curve of IPN2 film at room temperature (25 °C) was measured using the tensile machine by stretching the films along the nematic orientation direction as shown in Figure 2h. The Young's modulus of IPN2 at strain < 20% reaches 33.6 MPa and becomes 3.4 MPa at strain from 20% to 80%. Its breaking strength and strain are 8.8 MPa and 80%, respectively. The decrease of the Young's modulus at strain > 20% might be caused by the sacrificial rupture of one of the interpenetrating networks.[49] Despite this decrease, the mechanical properties of IPN2 are largely superior to the single ion-conducting LCE reported previously,[26] which possessed a Young's modulus of only 1.22 MPa and a breaking strength of 0.84 MPa at 75% strain, and was too soft to measure the actuation stress by any mechanical stress/strain sensor. We can conclude that the architectures of interpenetrating polymer networks do greatly improve the mechanical properties of ionic-conducting membrane IPN2. Since the actuation strain of IPN2 (9%) is below 20%, the mechanical characteristics below 20% strain are the most relevant. Until the linear strain of 20%, they are now in the range of mammalian skeletal muscles' values (Young's modulus of 10–60 MPa, actuation stress of 0.1–0.35 MPa and actuation strain of 20–40%).[31,32]

2.2. Trilayer Ionic Electroactive Device i-EAD-IPN-LCE as Actuator and Sensor

2.2.1. Mechanical and Thermal Mechanical Properties of i-EAD-IPN-LCE

To prepare trilayer i-EAD-IPN-LCE, the IPN2 film was first submitted to an annealing treatment (heating to 100 °C, then cooling down to 25 °C) to release the irreversible contraction as discussed above. The reversible contraction of annealed IPN2 as a function of temperature is shown in Figure S11 (Supporting Information). This IPN2 was coated on both sides with formulated PEDOT:PSS electrodes to get the trilayer i-EAD-IPN-LCE (PEDOT:PSS)/IPN2/(PEDOT:PSS) (see Scheme S2, Supporting Information). The elaboration procedure is detailed in SI. PEDOT:PSS was chosen as ECP due to its commercial availability, high conductivity, and ability to be casted directly on ion-conducting membranes. The ECP electrode formulation was composed of PEDOT:PSS (1.15 wt.% dispersion in H_2O), PEGDA, PEGMA, photo-initiator Irgacure 2959 and DMSO (Figure 1b). DMSO was added to promote the self-assembly of PEDOT into solid-state fibrillar structures that lead to excellent electrical conductivity.[50] An elastic network was formed by photo-polymerizing/cross-linking PEGDA and

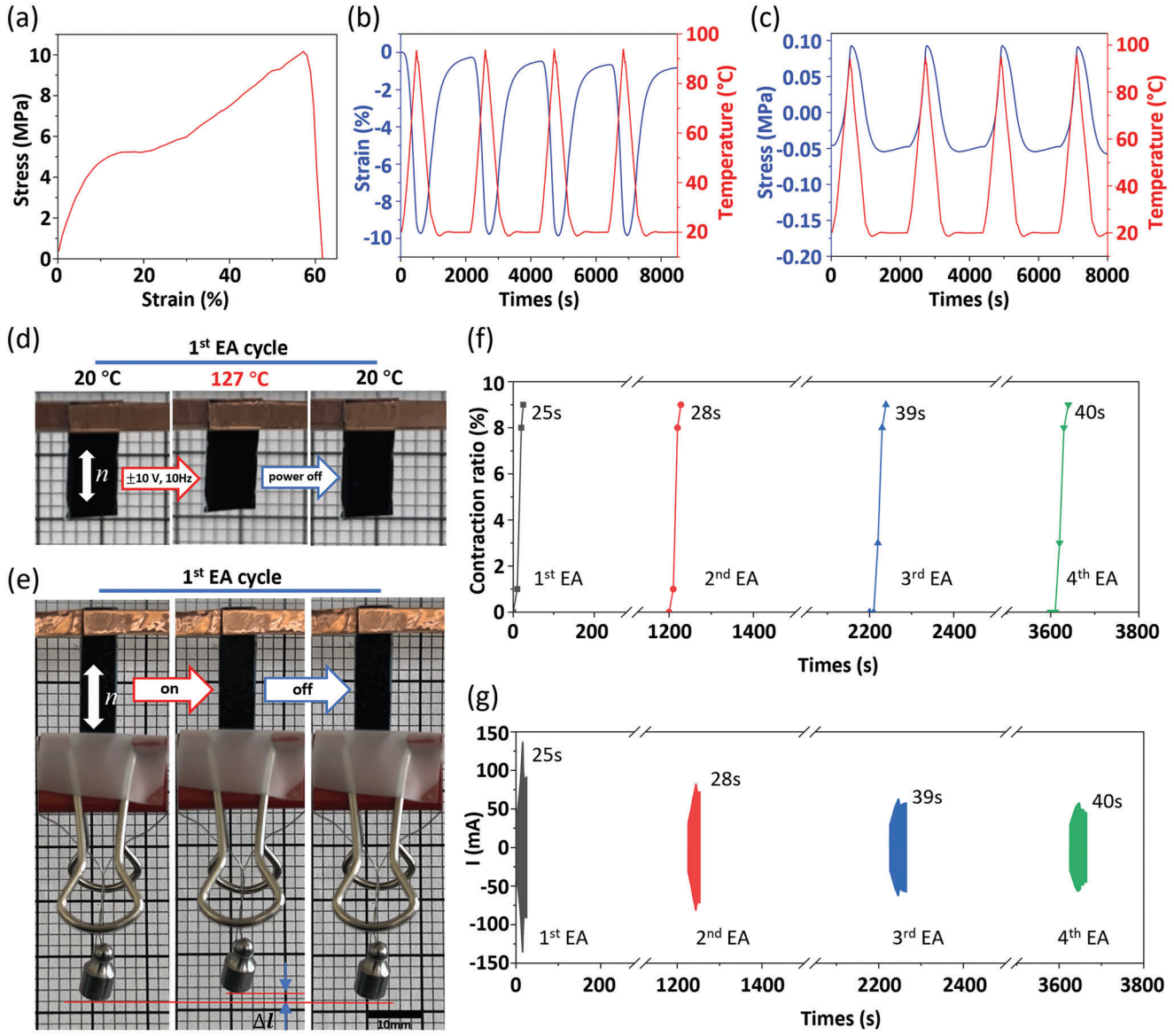

Figure 3. Mechanical and thermal mechanical properties of the i-EAD-IPN-LCE and its electroactive linear contraction under square wave potential (±10 V, 10 Hz). a) The stress-strain diagram measured at room temperature (strain rate:10 mm min^{-1}). b) Reversible thermal actuation strain measured at iso-stress mode by DMA (heating/cooling rate: ± 3 °C min^{-1}, stress control: 0.02 N). c) Thermal actuation stress measured at iso-strain mode by DMA (heating/cooling rate: ± 3 °C min^{-1}, strain control: 0.01% strain). d) Images of i-EAD-IPN-LCE film (black) without load upon the 1st electroactivation (EA) cycle with a maximal contraction ratio of 9%. e) Images of i-EAD-IPN-LCE film (black) with a load of 3.80 g upon 1st EA cycle, the load lift $\Delta l = 1.7$ mm. The mobile part of the film ($l \times h \times w = 18 \times 5.5 \times 0.57$ mm, scale bar = 10 mm) considered as the actuator weighs only 50 mg. f) Linear contraction ratio of i-EAD-IPN-LCE (without load) as a function of time during the power-on period of four EA cycles. The times to reach the maximal contraction are 25, 28, 39, and 40 s for the 1st, 2nd 3rd, and 4th EA, respectively. g) Current as a function of time during the power-on period of four EA cycles.

PEGMA to enhance the electrode mechanical properties. To evaluate the thickness of electrode, the same electrode was prepared on the glass slide surface in the same conditions. With a profilometer the thickness of the formulated PEDOT:PSS electrode was accurately measured as 8 µm. Therefore, the thickness of the two electrodes (16 µm) is only 3.1% of the i-EAD-IPN-LCE thickness, as the typical thickness of IPN2 is 500 µm. The electronic conductivity (σ_e) of the electrode was measured as 319 S cm^{-1} (see Supporting Information for detail).[28] Furthermore, the good thermal stability of the i-EAD-IPN-LCE was assessed by TGA with degradation onset temperature $T_{5\%}$ at 309 °C (Figure S10, Supporting Information).

The mechanical and thermal mechanical properties of the i-EAD-IPN-LCE were evaluated (**Figure 3a–c**). Its stress-strain diagram (Figure 3a) is different from that of the central membrane IPN2 (Figure 2h). After the first elastic zone at strain < 12%, two zones corresponding to yielding (12 – 22% strain) and rehardening (22 – 58% strain) are observed. Both regimes (Figures 2h and 3a) have already been reported for IPN.[49] Due to the

relatively higher modulus of formulated PEDOT:PSS electrode,[28] the Young's modulus of i-EAD-IPN-LCE increases to 51.6 MPa at strain < 12% and to 13.8 MPa at strain between 22% and 58%, while its breaking strength and strain are 10 MPa and 58%, respectively. On the other hand, the actuation strain of 9% and actuation stress of 0.14 MPa measured for i-EAD-IPN-LCE are similar to those of the central membrane IPN2 (see Table S4. Supporting Information).

2.2.2. i-EAD-IPN-LCE as a Linear Actuator

The electroactive linear contraction behaviors of i-EAD-IPN-LCE were first investigated. With the alternating ionic current, Joule effect can be produced by the movement of ions and to heat the IPN2 until N-I transition. Since the bending deformation became insignificant (< 0.06%) when the voltage frequency was above 10 Hz (see the discussion of bending deformation below), square potentials of ±5, ±6, ±7, ±8, ±9, and ±10 V at a constant frequency of 10 Hz were applied successively to test the electroactive contraction deformation of i-EAD-IPN-LCE. The contraction deformation could only be observed with voltage of ±10 V. Figure 3d,e shows the photographs of i-EAD-IPN-LCE without and with load, respectively, at starting and maximal contraction states under the 1st cycle of power on/off with electrical potential ±10 V at 10 Hz (see Figure S12a,b, Supporting Information for all the photographs of i-EAD-IPN-LCE under 1st to 4th cycles of power on/off). The temperature of i-EAD-IPN-LCE was recorded by a thermal camera. To ensure the temperature return to 20 °C, each power-off duration was 20 min. In the experiments without load, the contraction ratio and the current as a function of time during each power-on period (electroactivation) were also measured (Figure 3f,g). The maximum contraction ratios of 9% are confirmed for all four electroactuation (EA). The power-on times to reach the maximal contraction are 25, 28, 39, and 40 s for the 1st, 2nd, 3rd, and 4th EA, respectively (Figure 3f). Longer times are necessary for the 2nd, 3rd, and 4th EA to get the maximum contraction. This might be caused by the degradation of PEDOT upon the relatively high voltage (± 10 V). Indeed, the currents tend to reduce progressively from 1st to 4th EA (Figure 3g). Certainly, the applied potential of 10 V is still too high for the device. Work is in progress to develop new LCE membrane that has lower N-I phase transition temperature and thus needs lower electrical potential to activate.

The very fast actuation of the i-EAD-IPN-LCE is promising for potential applications as the heating rate reaches 250 °C min^{-1} in the 1st EA and 120 °C min^{-1} in the 4th EA. The work output performance was then evaluated in the experiment with load by hanging a 2 g counterpoise to the i-EAD-IPN-LCE film (Figure 3e). The total load (weights of the counterpoise and the clamp) was of 3.8 g. With the electroactive power input (±10 V, 10 Hz), the load of 3.8 g was lifted a distance Δl = 1.7 mm by the i-EAD-IPN-LCE film of 0.05 g (see Figure 3e; and Video S1, Supporting Information). In other words, a weight 76 times heavier than its own mass was lifted by doing a work of 6.3 × 10^{-5} J with a work capacity of 1.12 kJ m^{-3}. This work capacity is in the same order of magnitude as that of mammalian skeletal muscles (8 kJ m^{-3}).[31,32]

2.2.3. i-EAD-IPN-LCE as Bending Actuator and Sensor

The ability of the i-EAD-IPN-LCE to function as bending actuator and sensor was then examined. The principle of the electroactive bending deformation is illustrated in **Figure 4a**.[26] Typically, during the application of a potential difference (DC stimulation) between the two PEDOT:PSS electrodes, the oxidation (anode) of the already partially oxidized $PEDOT^{(x)+}$ into $PEDOT^{(x+y)+}$ will induce an expulsion of cations like $EMIM^+$ to keep the charge neutrality and will promote a volume contraction of the electrode. This ionic mechanism, i.e., the expulsion of cations instead of the insertion of anions, originates from both the higher mobility of $EMIM^+$ cations versus $TFSI^-$ anions[45] and the presence of PSS^- non-mobile macro-anions promoting cationic exchange. Concomitantly the reduction (cathode) of the $PEDOT^{(x)+}$ into $PEDOT^{(x-y)+}$ will promote the insertion of cations and the volume increase of the electrode. The combination of anode-shrinkage and cathode-expansion results in the trilayer film bending toward anode side. When the potential signs at the electrodes are reversed, an inverse bending deformation is obtained. By contrast, in the sensor mode, when applying mechanical bending force, the bending deformation creates a pressure gradient through the thickness of the ionic membrane from the compressed side to expanded side. Consequently, a pressure-induced flux of the electrolyte will be generated, promoting the transient separation of ionic charges with cations being faster than the anions and generating an open circuit voltage (OCV) variation as electrical signal output.[28,51,52]

For the bending actuation, a square potential ±2 V at 0.1 Hz was first used as stimulus.[26] Unfortunately, no bending deformation was observed, probably because the ionic conductivity of IPN2 (3.4 × 10^{-5} S cm^{-1} at 20 °C) is an order of magnitude smaller than that of LCE reported previously (1.0 × 10^{-4} S cm^{-1} at 20 °C).[26] Then, higher voltages of ±3, ±4, and ±5 V at 0.1 Hz were tested, and the electroactive redox process of i-EAD-IPN-LCE was also analyzed by cyclic voltammetry (CV) (Figure S13, Supporting Information). The bending deformation was only observed with ±5 V as shown in Figure 4b (see also Video S2, Supporting Information). As an example of bending actuator, i-EAD-IPN-LCE (0.08 g) can kick a small ball of 0.41 g to a certain distance to mimic the golf shot (Figure 4c). Thus, i-EAD-IPN-LCE successfully converts the electrical energy into the mechanical motion (Video S3, Supporting Information). The current as a function of time and the real-time mechanical bending responses recorded by the laser displacement sensor are shown in Figure 4d,e, respectively. For a 0.59 mm-thick i-EAD-IPN-LCE, the maximum peak-to-peak displacement at L = 5 mm was D = 0.5 mm as schematically illustrated in Figure 4f (see also Scheme S3, Supporting Information) under the electrical stimulation of ±5 V at 0.1 Hz. The bending deformation was normally quantified by the bending strain difference between the two electrodes, $\Delta\epsilon = \frac{2D\times w}{D^2+L^2}$, here the maximal $\Delta\epsilon$ being 1.18% for i-EAD-IPN-LCE (see Supporting Information for detail).[46] Under ±5 V at higher frequencies (1.25, 5, 10, and 20 Hz), the bending strain difference were also assessed, which decreased rapidly with increasing frequency as expected for an actuation process controlled by ionic movements. As shown in Figure S14 (Supporting Information), $\Delta\epsilon$ became negligeable (0.06%) at 10 Hz. That is why in the above discussion about linear contraction of

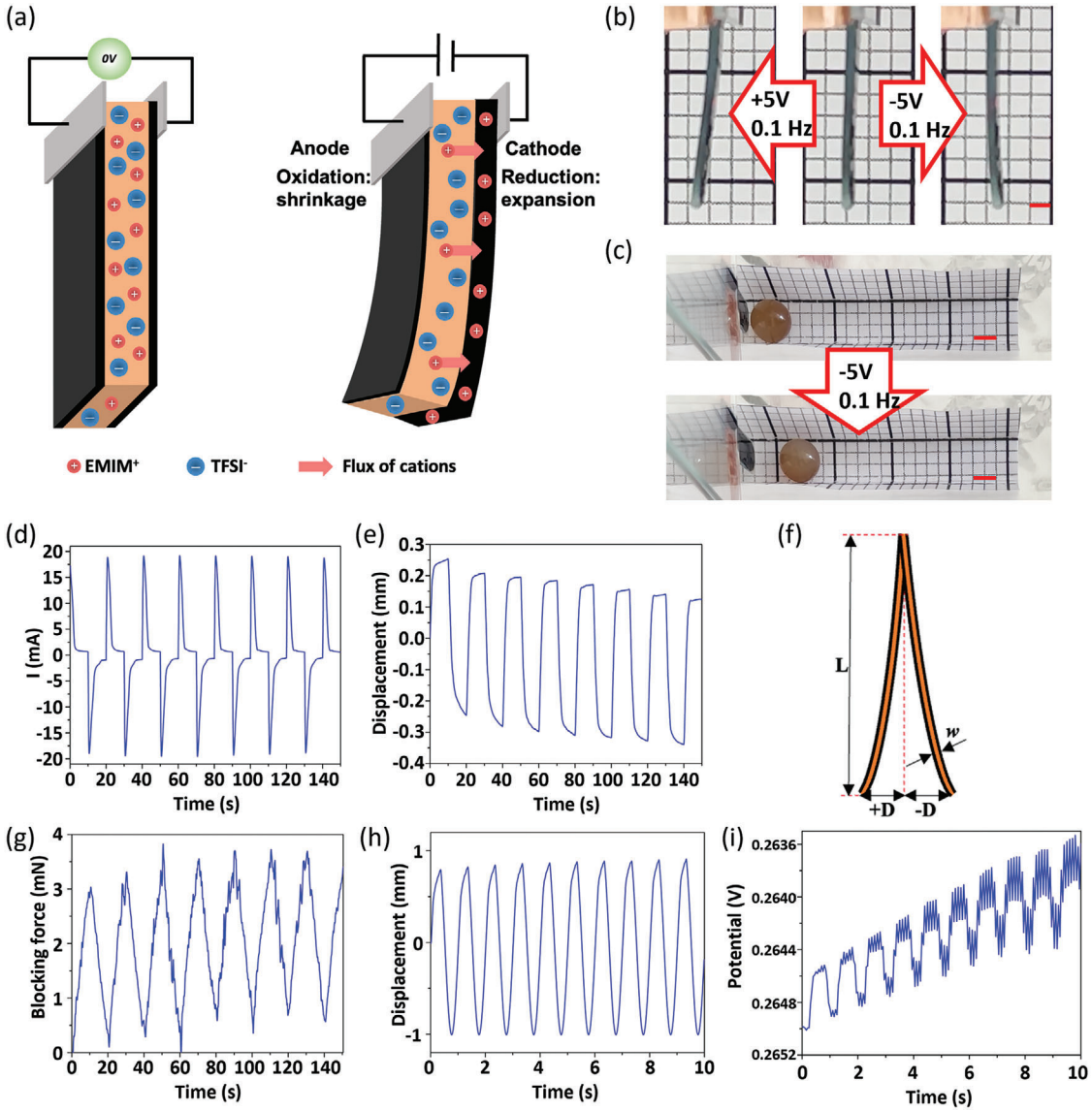

Figure 4. a) Schematic illustration of the principle of electroactive bending. b) Images of bending deformation (scale bar = 2 mm) of i-EAD-IPN-LCE (sample thickness $w = 0.59$ mm) under electrical stimulation of square wave potential ±5 V at 0.1 Hz. c) Golf shot mimicry by the output force of the bending deformation (top view, scale bar = 4 mm). d) Temporal measurement of currents. e) Temporal measurement of displacements recorded by a laser sensor placed at L = 5 mm (see Scheme S3, Supporting Information). f) Illustration of key parameters to calculate the bending strain difference $\Delta\epsilon$. g) Temporal measurement of blocking force of i-EAD-IPN-LCE ($w = 0.51$ mm) made at L = 3 mm under ±5 V at 0.1 Hz. h) A sinusoidal displacement of ± 1 mm at 1 Hz for testing the i-EAD-IPN-LCE as a bending sensor. The tip of the lever arm was in contact with i-EAD-IPN-LCE ($w = 0.51$ mm) at the distance of L = 3 mm from the clamped side. The mechanical bending of a strain difference of 9% was finally applied to the i-EAD-IPN-LCE sample. i) Open Circuit Voltage response to the mechanical bending.

i-EAD-IPN-LCE, potentials applied were at 10 Hz. The blocking force of the i-EAD-IPN-LCE sample was also measured under ±5 V at 0.1 Hz at L = 3 mm (see Supporting Information for detail), the output force reaching 3 mN as shown in Figure 4g. The bending strain difference (1.18%) and output force (3 mN) of i-EAD-IPN-LCE are comparable to the values published in the literature (see Table S5, Supporting Information).[28,29,45,46,53]

Finally, the i-EAD-IPN-LCE as a sensor was studied using a lever arm system to apply mechanical displacement and a multichannel potentiostat to record OCV (see Supporting Information for detail). The tip of lever arm was placed at the distance L = 3 mm from the fixed side of the sample; the two PEDOT:PSS electrodes were connected to the working and reference electrodes of the potentiostat (see Scheme S4, Supporting Information). With a force of 100 mN, the sinusoidal displacement of the lever arm was set as ± 1 mm at 1 Hz (Figure 4h). The bending strain difference thus applied was 9%. During upward bending, the top PEDOT:PSS electrode was compressed, while during downward bending the down electrode was compressed. Consequently, an output voltage signal of 0.4 mV was produced (Figure 4i) due to the pressure-induced transient separation of ionic charges as discussed above. This exciting result represents

one of the rare examples of ionic LCE systems capable of detecting mechanical stimulation and transferring it into electrical signals.[15,54]

3. Conclusion

In this work, we have elaborated a trilayer ionic electroactive device i-EAD-IPN-LCE with interpenetrating liquid crystal elastomer and ionogel as the central ion-conducting membrane. Compared to the previously reported i-EAD-LCE with a single ion-conducting LCE, the architecture of interpenetrating polymer networks allows to improve greatly the mechanical properties of the device. This i-EAD-IPN-LCE with a typical thickness of 0.5 mm can function not only as linear and bending actuators, but also as a bending sensor. It can perform selectively either bending deformation or linear contraction by controlling electrical stimulation of low voltages (±5 V at 0.1 Hz or ±10 V at 10 Hz). As a linear actuator, its Young's modulus, actuation stress and actuation strain are 51.6 MPa, 0.14 MPa and 9%, respectively, reaching mammalian skeletal muscles' values. By contrast, the previous device i-EAD-LCE has a Young's modulus of only 1.63 MPa. As a bending actuator, the i-EAD-IPN-LCE exhibits a bending strain difference ($\Delta\epsilon$) of 1.18% with an output force of 3 mN. It can also operate as a sensor producing 0.4 mV Open Circuit Voltage in response to bending deformation of $\Delta\epsilon = 9\%$. In conclusion, this i-EAD-IPN-LCE is a promising system for the fabrication of robust electroactive devices and sensors with multiple degrees of freedom.

4. Experimental Section

Experimental details are given in the Supporting Information.

Supporting Information

Supporting Information is available from the Wiley Online Library or from the author.

Acknowledgements

Y.D. and G.L. contributed equally to this work. This work was financially supported by the French National Research Agency (ANR-22-CE06-0023, AS-LCE). The China Scholarship Council (CSC) is gratefully acknowledged by Y.D. and G.L. for funding their Ph.D. scholarships.

Conflict of Interest

The authors declare no conflict of interest.

Data Availability Statement

The data that support the findings of this study are available in the supplementary material of this article.

Keywords

bending deformation, electroactive actuator, interpenetrating polymer network (IPN), linear contraction, liquid crystal elastomer (LCE), mechanical sensor, thermal actuation

Received: March 4, 2024
Revised: April 12, 2024
Published online:

[1] Z. Shen, F. Chen, X. Zhu, K. T. Yong, G. Gu, *J. Mater. Chem. B* **2020**, *8*, 8972.
[2] X. Xia, C. M. Spadaccini, J. R. Greer, *Nat. Rev. Mater.* **2022**, *7*, 683.
[3] M. H. Li, P. Keller, *Phil. Trans. R. Soc. A* **2006**, *364*, 2763.
[4] C. Ohm, M. Brehmer, R. Zentel, *Adv. Mater.* **2010**, *22*, 3366.
[5] T. J. White, D. J. Broer, *Nat. Mater.* **2015**, *14*, 1087.
[6] S. W. Ula, N. A. Traugutt, R. H. Volpe, R. R. Patel, K. Yu, C. M. Yakacki, *Liq. Cryst. Rev.* **2018**, *6*, 78.
[7] M. H. Li, P. Keller, J. Yang, P. A. Albouy, *Adv. Mater.* **2004**, *16*, 1922.
[8] B. Ni, G. Liu, M. Zhang, P. Keller, M. Tatoulian, M. H. Li, *CCS Chem.* **2022**, *4*, 847.
[9] Y. Wang, J. Sun, W. Liao, Z. Yang, *Adv. Mater.* **2022**, *34*, 2107840.
[10] A. Potekhina, C. Wang, *Adv. Mater. Technol.* **2022**, *7*, 2101732.
[11] J. Hu, Z. Nie, M. Wang, Z. Liu, S. Huang, H. Yang, *Angew. Chem., Int. Ed.* **2023**, *62*, 202218227.
[12] M. H. Li, P. Keller, B. Li, X. Wang, M. Brunet, *Adv. Mater.* **2003**, *15*, 569.
[13] T. Ube, T. Ikeda, *Angew. Chem., Int. Ed.* **2014**, *53*, 10290.
[14] H. Zeng, O. M. Wani, P. Wasylczyk, R. Kaczmarek, A. Priimagi, *Adv. Mater.* **2017**, *29*, 1701814.
[15] X. Zheng, Y. Jia, A. Chen, *Nat. Commun.* **2021**, *12*, 4875.
[16] X. Huang, L. Qin, J. Wang, X. Zhang, B. Peng, Y. Yu, *Adv. Funct. Mater.* **2022**, *32*, 2208312.
[17] P.-G. de Gennes, *CR Acad. Sci. Paris, Ser. B* **1975**, *281*, 101.
[18] M. Hébert, R. Kant R, P.-G. de Gennes, *J. Phys. I* **1997**, *7*, 909.
[19] J. P. Cotton, F. Hardouin, *Prog. Polym. Sri.* **1997**, *22*, 795.
[20] K. M. Herbert, H. E. Fowler, J. M. McCracken, K. R. Schlafmann, J. A. Koch, T. J. White, *Nat. Rev. Mater.* **2022**, *7*, 23.
[21] M. Mohiuddin, T. T. Tung, in *Flexible and Stretchable Electronic Composites. Springer Series on Polymer and Composite Materials*, Springer, Cham **2016**, Ch. 13.
[22] S. Schuhladen, F. Preller, R. Rix, S. Petsch, R. Zentel, H. Zappe, *Adv. Mater.* **2014**, *26*, 7247.
[23] C. Wang, K. Sim, J. Chen, H. Kim, Z. Rao, Y. Li, W. Chen, J. Song, R. Verduzco, C. Yu, *Adv. Mater.* **2018**, *30*, 1706695.
[24] M. J. Ford, M. Palaniswamy, C. P. Ambulo, T. H. Ware, C. Majidi, *Soft Matter* **2020**, *16*, 5878.
[25] J. Sun, Y. Wang, W. Liao, Z. Yang, *Small* **2021**, *17*, 2103700.
[26] G. Liu, Y. Deng, B. Ni, G. T. M. Nguyen, C. Vancaeyzeele, A. Brûlet, F. Vidal, C. Plesse, M.-H. Li, *Small* **2024**, *20*, 2307565.
[27] H. Okuzaki, S. Takagi, F. Hishiki, R. Tanigawa, *Sens. Actuators, B* **2014**, *194*, 59.
[28] K. Rohtlaid, G. T. M. Nguyen, C. Soyer, E. Cattan, F. Vidal, C. Plesse, *Adv. Electron. Mater.* **2019**, *5*, 1800948.
[29] K. Rohtlaid, G. T. M. Nguyen, S. Ebrahimi-Takalloo, T. N. Nguyen, J. D. W. Madden, F. Vidal, C. Plesse, *Adv. Mater. Technol.* **2021**, *6*, 2001063.
[30] J. G. Martinez, C. Plesse, F. Vidal, W. Zheng, in *Electromechanically Active Polymers: A Concise Reference*, (Ed: F. Carpi), Springer International Publishing, Cham **2016**.
[31] J. D. W. Madden, N. A. Vandesteeg, P. A. Anquetil, P. G. A. Madden, A. Takshi, R. Z. Pytel, S. R. Lafontaine, P. A. Wieringa, I. W. Hunter, *IEEE J. Oceanic Eng.* **2004**, *29*, 706.
[32] S. M. Mirvakili, I. W. Hunter, *Adv. Mater.* **2018**, *30*, 1704407.
[33] J. P. Gong, Y. Katsuyama, T. Kurokawa, Y. Osada, *Adv. Mater.* **2003**, *15*, 1155.
[34] T. Matsuda, R. Kawakami, R. Namba, T. Nakajima, J. P. Gong, *Science* **2019**, *363*, 504.
[35] Y. Zhao, G. Yuan, *Macromolecules* **1996**, *29*, 1067.

[36] Y. Zhao, G. Yuan, P. Roche, *Polymer* **1999**, *40*, 3025.
[37] T. Ube, K. Takado, T. Ikeda, *J. Mater. Chem. C* **2015**, *3*, 8006.
[38] T. Ube, K. Minagawa, T. Ikeda, *Soft Matter* **2017**, *13*, 5820.
[39] J. E. Stumpel, E. R. Gil, A. B. Spoelstra, C. W. M. Bastiaansen, D. J. Broer, A. P. H. J. Schenning, *Adv. Funct. Mater.* **2015**, *25*, 3314.
[40] G. A. Becht, M. Sofos, S. Seifert, M. A. Firestone, *Macromolecules* **2011**, *44*, 1421.
[41] K.-G. Noh, S.-Y. Park, *Adv. Funct. Mater.* **2018**, *28*, 1707562.
[42] H. F. Lu, M. Wang, X. M. Chen, B. P. Lin, H. Yang, *J. Am. Chem. Soc.* **2019**, *141*, 14364.
[43] R. Annapooranan, Y. Wang, S. Cai, *ACS Appl. Mater. Interfaces* **2022**, *14*, 2006.
[44] L. Li, X. Dong, M. Li, Y. Jiang, J. Xu, Q. Li, N. Yuan, J. Ding, *Sens. Actuator, A* **2023**, *349*, 114069.
[45] N. Festin, A. Maziz, C. Plesse, D. Teyssié, C. Chevrot, F. Vidal, *Smart Mater. Struct.* **2013**, *22*, 104005.
[46] A. Maziz, C. Plesse, C. Soyer, C. Chevrot, D. Teyssié, E. Cattan, F. Vidal, *Adv. Funct. Mater.* **2014**, *24*, 4851.
[47] A. Khaldi, C. Plesse, F. Vidal, S. K. Smoukov, *Adv. Mater.* **2015**, *27*, 4418.
[48] M. Deutsch, *Phys. Rev. A* **1991**, *44*, 8264.
[49] Y. Tanaka, Y. Kawauchi, T. Kurokawa, H. Furukawa, T. Okajima, J. P. Gong, *Macromol. Rapid Commun.* **2008**, *29*, 1514.
[50] E. Dauzon, A. E. Mansour, M. R. Niazi, R. Munir, D. M. Smilgies, X. Sallenave, C. Plesse, F. Goubard, A. Amassian, *ACS Appl. Mater. Interfaces* **2019**, *11*, 17570.
[51] Y. Dobashi, D. Yao, Y. Petel, T. N. Nguyen, M. S. Sarwar, Y. Thabet, C. L. W. Ng, E. S. Glitz, G. T. M. Nguyen, C. Plesse, F. Vidal, C. A. Michal, J. D. W. Madden, *Science* **2022**, *376*, 502.
[52] D. Ho, *ChemElectroChem* **2024**, *11*, 202300268.
[53] C. Liu, S. Cao, M. Yoshio, *Adv. Funct. Mater.* **2023**, *33*, 2300538.
[54] A. Alyami, C. P. H. Rajapaksha, P. R. Paudel, V. Kaphle, S. G. Kodikara, B. Lüssem, A. Jákli, *Liq. Cryst.* **2024**, *51*, 297.